Inorg. Chem. **2006**, *45*, 582–590

Syntheses, Structures, and Magnetic Properties of Cyano-Bridged Heterobimetallic Complexes Based on $[Fe(bpca)(CN)_3]^-$

He-Rui Wen,[†] Cai-Feng Wang,[†] Jing-Lin Zuo,*[,†] You Song,*[,†] Xi-Rui Zeng,[‡] and Xiao-Zeng You[†]

Coordination Chemistry Institute, State Key Laboratory of Coordination Chemistry, Nanjing University, Nanjing 210093, P. R. China, and Department of Chemistry, JingGangShan Normal College, Jian 343009, P. R. China

Received July 11, 2005

Two new cyano-bridged one-dimensional heterobimetallic coordination polymers, $[(bpca)_2Fe^{III}_2(CN)_6Cu(H_2O)_2\cdot 1.5H_2O]_n$ (**2**) and $[(bpca)Fe^{III}(CN)_3Cu(bpca)(H_2O)\cdot H_2O]_n$ (**3**), and a trinuclear complex, $[(bpca)_2Fe^{III}_2(CN)_6Mn(CH_3OH)_2(H_2O)_2]\cdot 2H_2O$ (**4**), have been synthesized using the tailored tricyanometalate precursor $(Bu_4N)[Fe(bpca)(CN)_3]\cdot H_2O$ (**1**) (Bu_4N^+ = tetrabutylammonium cation; bpca = bis(2-pyridylcarbonyl)amidate anion) as a building block and structurally characterized. In complex **2**, the Cu^{II} ions are six-coordinated in an elongated distorted octahedral environment, and they are linked by distorted octahedrons of $[Fe(bpca)(CN)_3]^-$ to form 1D chain of squares. Complex **3** is an unexpected chiral heterobimetallic helical chain complex, in which the helical chain consists of the asymmetric unit of $[(bpca)Fe(CN)_3Cu(bpca)(H_2O)]$. In complex **4**, there are two independent trinuclear clusters in one asymmetric unit, and the coordination modes of the two methanol and two water molecules coordinating to the central Mn(II) ion are different (cis and trans). Complex **2** shows metamagnetic behavior with a Neel temperature of $T_N = 2.2$ K and a critical field of 250 Oe at 1.8 K, where the cyanides mediate the intrachain ferromagnetic coupling between the Cu^{II} and Fe^{III} ions. Complex **3** shows ferromagnetic coupling between Cu^{II} and Fe^{III} ions, the best-fit for $\chi_M T$ versus T using a 1D alternating chain model leads to the parameters $J_1 = 7.9(3)$ cm^{-1}, $J_2 = 1.03(2)$ cm^{-1}, and $g = 2.196(3)$. Complex **4** exhibits ferrimagnetic behavior caused by the noncompensation of the local interacting spins ($S_{Mn} = 5/2$ and $S_{Fe} = 1/2$) which interact antiferromagnetically through bridging cyano groups.

Introduction

The cyano-bridged bimetallic assemblies of Prussian Blue type have been intensively studied over the past decade because of their rich magnetic behavior,[1] including high-T_c magnetism,[2] photo- and electro-magnetism,[3] and single-molecule[4] or single-chain magnetism.[5] However, the application of three-dimensional Prussian Blue analogues obtained using a stable hexacyanometallic anion, $[M(CN)_6]^{n-}$, as building block toward fully solvated transition metal ions was limited because of their insolubility and difficulty in producing single crystals. If the second transition metal ions are partially blocked with organic polydentate ligands, some interesting lower-dimensional heterobimetallic compounds with very different topologies and structures have been obtained.[6−8] Since Rikken and Raupach observed the weak magneto-chiral dichroism (MChD) effect in a chiral paramagnetic material,[9] the investigation of chiral magnets combining magnetism and optical activity has become an active topic for its important potential application as mul-

* To whom correspondence should be addressed. Email: zuojl@nju.edu.cn. Fax: +86-25-83314502.

[†] Nanjing University.

[‡] JingGangShan Normal College.

(1) (a) Entley, W. R.; Girolami, G. S. *Science* **1995**, *268*, 397−400. (b) Dunbar, K. R.; Heintz, R. A. *Prog. Inorg. Chem.* **1997**, *45*, 2283−391. (c) Verdaguer, M.; Bleuzen, A.; Marvaud, V.; Vaissermann, J.; Seuleiman, M.; Desplanches, C.; Scuiller, A.; Train, C.; Garde, R.; Gelly, G.; Lomenech, C.; Rosenman, I.; Veillet, P.; Cartier, C.; Villain, F. *Coord. Chem. Rev.* **1999**, *190−192*, 1023−1047. (d) Ohba, M.; Ôkawa, H. *Coord. Chem. Rev.* **2000**, *198*, 313−328. (e) Èernak, J.; Orendaè, M.; Potoèòak, I.; Chomiè, J.; Orendaèová, A.; Skor×f0epa, J.; Feher, A. *Coord. Chem. Rev.* **2002**, *224*, 51−66. (f) Beltran, L. M. C.; Long, J. R. *Acc. Chem. Res.* **2005**, *38*, 325−334.

(2) (a) Ferlay, S.; Mallah, T.; Quahès, R.; Veillet, P.; Verdaguer, M. *Nature* **1995**, *378*, 701−703. (b) Sato, O.; Iyoda, T.; Fujishima, A.; Hashimoto, K. *Science* **1996**, *271*, 49−51. (c) Holmes, S. M.; Girolami, G. S. *J. Am. Chem. Soc.* **1999**, *121*, 5593−5594. (d) Hatlevik, Ø.; Buschman, W. E.; Zhang, J.; Manson, J. L.; Miller, J. S. *Adv. Mater.* **1999**, *11*, 914−918.

(3) (a) Sato, O.; Iyoda, T.; Fujishima, A.; Hashimoto, K. *Science* **1996**, *272*, 704−705. (b) Ohkoshi, S. I.; Fujishima, A.; Hashimoto, K. *J. Am. Chem. Soc.* **1998**, *120*, 5349−5350. (c) Sato, O.; Einaga, Y.; Fujishima, A.; Hashimoto, K. *Inorg. Chem.* **1999**, *38*, 4405−4412. (d) Shimamoto, N.; Ohkoshi, S. I.; Sato, O.; Hashimoto, K. *Inorg. Chem.* **2002**, *41*, 678−684. (e) Yokoyama, T.; Okamoto, K.; Ohta, T.; Ohkoshi, S. I.; Hashimoto, K. *Phys. Rev. B* **2002**, *65*, 064438−064446. (f) Arimoto, Y.; Ohkoshi, S. I.; Zhong, Z. J.; Seino, H.; Mizobe, Y.; Hashimoto, K. *J. Am. Chem. Soc.* **2003**, *125*, 9240−9241. (g) Sato, O. *Acc. Chem. Res.* **2003**, *36*, 692−700 and references therein.

10.1021/ic0511468 CCC: $33.50
Published on Web 12/24/2005

tifunctional material.[10] To date, several examples of cyano-bridged chiral ferromagnetic compounds with hexacyanometallic anions and transition metal ions partially blocked by organic chiral diamine ligands have been reported.[11]

Recently, synthetic strategies to prepare cyano-bridged bimetallic systems using modified cyanometalates, $[M(L)_y(CN)_x]^{(x-m)-}$ (M = first row transition metallic ions and L = organic polydentate ligands), as multidentate ligands and linkers were developed. The following are representative examples: $[M(phen)(CN)_4]^-$, $[M(bipy)(CN)_4]^-$ (M = Cr^{3+}, Fe^{3+}, phen = 1,10-phenanthroline; bipy = 2,2′-bipyridine),[12] $[(tacn)M(CN)_3]$ (M = Co^{3+}, Cr^{3+}; tacn = 1,4,7-triazacyclononane),[13] $[(tach)M(CN)_3]$ (M = Cr^{3+}, Fe^{3+}, Co^{3+}; tach = 1,3,5-triaminocyclohexane),[14] $[(Me_3tacn)M(CN)_3]$ (M = Cr^{3+}, Mo^{3+}; Me_3tacn = *N*, *N*′, *N*″-trimethyl-1,4,7-triazacyclononane),[15] $[(Tp)Fe(CN)_3]^-$ (Tp = hydrotris(pyrazolyl)-borate),[4,5,16] and $[CpM(CN)_3]^-$ (M = Co^{3+}, Cp = cyclopentadienyl; M = Rh^{3+}, Ir^{3+}, Cp* = 1,2,3,4,5-pentamethylcyclopentadienyl).[17] On the basis of these building blocks, some heterobimetallic complexes exhibiting interesting structures and magnetic properties were synthesized,[4,5,12−18] including several single-molecule magnets (SMMs)[4f,4g] and single-chain magnets (SCMs)[5] which are possibly useful for information storage and computer science.

Scheme 1[a]

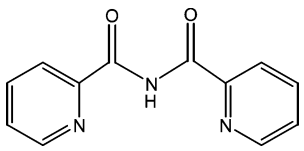

[a] Hbpca = bis(2-pyridylcarbonyl)amide

As part of an effort to develop new examples of cyano-bridged heterobimetallic magnetic complexes, we chose another tricyanometalate precursor, $[Fe(bpca)(CN)_3]^-$ (bpca = bis(2-pyridylcarbonyl)amidate anion, Scheme 1), to synthesize new low-dimensional cyano-bridged magnetic compounds. Both Tp and bpca bear a negative charge, but Tp is a classical scorpionate ligand with a C_3 axis and the bpca ligand is planar. Lescouëzec et al. have used $[Fe(bpca)(CN)_3]^-$ as precursor to prepare a ladderlike chain compound, $[Fe(bpca)(\mu\text{-}CN)_3Mn(H_2O)_3]_n^{n+}$.[19] Herein, we report the syntheses, crystal structures, and magnetic properties of two new cyano-bridged one-dimensional heterobimetallic coordination polymers based on $[Fe(bpca)(CN)_3]^-$, $[(bpca)_2Fe^{III}_2(CN)_6Cu(H_2O)_2\cdot 1.5H_2O]_n$ (**2**), and $[(bpca)Fe^{III}(CN)_3Cu(bpca)(H_2O)\cdot H_2O]_n$ (**3**), and a trinuclear complex, $[(bpca)_2Fe^{III}_2(CN)_6Mn$-

(4) (a) Sokol, J. J.; Hee A. G.; Long, J. R. *J. Am. Chem. Soc.* **2002**, *124*, 7656−7657. (b) Berlinguette, C. P.; Vaughn, D.; Cañada-Vilalta, C.; Galán-Mascarós, J. R.; Dunbar, K. R. *Angew. Chem., Int. Ed.* **2003**, *42*, 1523−1526. (c) Mironov, V. S.; Chibotaru, L. F.; Ceulemans, A. *J. Am. Chem. Soc.* **2003**, *125*, 9750−9760. (d) Choi, H. J.; Sokol, J. J.; Long, J. R. *Inorg. Chem.* **2004**, *43*, 1606−1608. (e) Schelter, E. J.; Prosvirin, A. V.; Dunbar, K. R. *J. Am. Chem. Soc.* **2004**, *126*, 15004−15005. (f) Wang, S.; Zuo, J. L.; Zhou, H. C.; Choi, H. J.; Ke, Y.; Long, J. R.; You, X. Z. *Angew. Chem., Int. Ed*. **2004**, *43*, 5940−5943. (g) Li, D.; Parkin, S.; Wang, G.; Yee, G. T.; Prosvirin, A. V.; Holmes, S. M. *Inorg. Chem.* **2005**, *44*, 4903−4905.

(5) (a) Lescouëzec, R.; Vaissermann, J.; Ruiz-Pérez, C.; Lloret, F.; Carrasco, R.; Julve, M.; Verdaguer, M.; Dromzee, Y.; Gatteschi, D.; Wernsdorfer, W. *Angew. Chem., Int. Ed.* **2003**, *42*, 1483−1486. (b) Toma, L. M.; Lescouëzec, R.; Lloret, F.; Julve, M.; Vaissermann, J.; Verdaguer, M. *Chem. Commun.* **2003**, 1850−1851. (c) Wang, S.; Zuo, J. L.; Gao, S.; Song, Y.; Zhou, H. C.; Zhang, Y. Z.; You, X. Z. *J. Am. Chem. Soc.* **2004**, *126*, 8900−8901.

(6) (a) Parker, R. J.; Hockless, D. C. R.; Moubaraki, B.; Murray, K. S.; Spiccia, L. *Chem. Commun.* **1996**, 2789−2790. (b) Ferlay, S.; Mallah, T.; Vaissermann, J.; Bartolomé, F.; Veillet, P.; Verdaguer, M. *Chem. Commun*. **1996**, 2481−2482. (c) Colacio, E.; Domínguez-Vera, J. M.; Ghazi, M.; Kivekäs, R.; Klinga, M.; Moreno, J. M. *Chem. Commun*. **1998**, 1071−1072. (d) EI Fallah, M. S.; Ribas, J.; Solans, X.; Font-Bardia, M. *J. Chem. Soc., Dalton Trans*. **2001**, 247−250. (e) Parker, R. J.; Spiccia, L.; Berry, K. J.; Fallon, G. D.; Moubaraki, B.; Murray, K. S. *Chem. Commun*. **2001**, 333−334.

(7) (a) Miyasaka, H.; Matsumoto, N.; Ôkawa, H.; Re, N.; Gallo, E.; Floriani, C. *J. Am. Chem. Soc*. **1996**, *118*, 981−994. (b) Miyasaka, H.; Ieda, H.; Matsumoto, N.; Re, N.; Crescenzi, R.; Floriani, C. *Inorg. Chem.* **1998**, *37*, 255−263.

(8) (a) Marvaud, V.; Decroix, C.; Scuiller, A.; Guyard-Duhayon, C.; Vaissermann, J.; Gonnet, F.; Verdaguer, M. *Chem.*−*Eur. J*. **2003**, *9*, 1677−1691. (b) Marvaud, V.; Decroix, C.; Scuiller, A.; Tuyèras, F.; Guyard-Duhayon, C.; Vaissermann, J.; Marrot, J.; Gonnet, F.; Verdaguer, M. *Chem.*−*Eur. J.* **2003**, *9*, 1692−1705.

(9) Rikken, G. L. J. A.; Raupach, E. *Nature* **1997**, *390*, 493−494.

(10) (a) Kumagai, H.; Inoue, K. *Angew. Chem., Int. Ed*. **1999**, *38***,** 1601−1603. (b) Minguet, M.; Luneau, D.; Lhotel, E.; Villar, V.; Paulsen, C.; Amabilino, D. B.; Veciana, J. *Angew. Chem., Int. Ed.* **2002**, *41***,** 586−589. (c) Gao, E. Q.; Yue, Y. F.; Bai, S. Q.; He, Z.; Yan, C. H. *J. Am. Chem. Soc.* **2004**, *126***,** 1419−1429. (d) Liu, W. L.; Song, Y.; Li, Y. Z.; Zou, Y.; Dang, D. B.; Ni, C. L.; Meng, Q. J. *Chem. Commun.* **2004**, 2348−2349. (e) Coronado, E.; Palacio, F.; Veciana, J. *Angew. Chem., Int. Ed.* **2003**, *42*, 2570−2572.

(11) (a) Inoue, K.; Imai, H.; Ghalsasi, P. S.; Kikuchi, K.; Ohba, M.; Ôkawa, H.; Yakhmi, J. V. *Angew. Chem., Int. Ed.* **2001**, *40*, 4242−4245. (b) Coronado, E.; Gómez-García, C. J.; Nuez, A.; Romero, F. M.; Rusanov, E.; Stoeckli-Evans, H. *Inorg. Chem*. **2002**, *41*, 4615−4617. (c) Inoue, K.; Kikuchi, K.; Ohba, M.; Ôkawa, H. *Angew. Chem., Int. Ed.* **2003**, *42*, 4810−4813. (d) Imai, H.; Inoue, K.; Kikuchi, K.; Yoshida, Y.; Ito, M.; Sunahara, T.; Onaka, S. *Angew. Chem., Int. Ed.* **2004**, *43***,** 5618−5621.

(12) (a) Lescouëzec, R.; Lloret, F.; Julve, M.; Vaissermann, J.; Verdaguer, M.; Llusar, R.; Uriel, S. *Inorg. Chem.* **2001**, *40*, 2065−2072. (b) Lescouëzec, R.; Lloret, F.; Julve, M.; Vaissermann, J.; Verdaguer, M. *Inorg. Chem*. **2002**, *41*, 818−826. (c) Toma, L.; Lescouëzec, R.; Vaissermann, J.; Delgado, F. S.; Ruiz-Pérez, C.; Carrasco, R.; Cano, J.; Lloret, F.; Julve, M. *Chem.*−*Eur. J*. **2004**, *10*, 6130−6145. (d) Toma, L. M.; Delgado, F. S.; Ruiz-Pérez, C.; Carrasco, R.; Cano, J.; Lloret, F.; Julve, M. *J. Chem. Soc., Dalton Trans.* **2004**, 2836−2846. (e) Zhang, Y. Z.; Gao, S.; Wang, Z. M.; Su, G.; Sun, H. L.; Pan, F. *Inorg. Chem*. **2005**, *44*, 4534−4545. (f) Toma, L.; Toma, L. M.; Lescouëzec, R.; Armentano, D.; Munno, G. D.; Andruh, M.; Cano, J.; Lloret, F.; Julve, M. *J. Chem. Soc., Dalton Trans*. **2005**, 1357−1364.

(13) Heinrich, J. L.; Berseth, P. A.; Long, J. R. *Chem. Commun.* **1998**, 1231−1232.

(14) Sokol, J. J.; Shores, M. P.; Long, J. R. *Angew. Chem., Int. Ed*. **2001**, *40*, 236−239.

(15) (a) Berseth, P. A.; Sokol, J. J.; Shores, M. P.; Heinrich, J. L.; Long, J. R. *J. Am. Chem. Soc*. **2000**, *122*, 9655−9662. (b) Shores, M. P.; Sokol, J. J.; Long, J. R. *J. Am. Chem. Soc*. **2002**, *124*, 2279−2292. (c) Yang, J. Y.; Shores, M. P.; Sokol, J. J.; Long, J. R. *Inorg. Chem*. **2003**, *42*, 1403−1419.

(16) (a) Lescouëzec, R.; Vaissermann, J.; Lloret, F.; Julve, M.; Verdaguer, M. *Inorg. Chem*. **2002**, *41*, 5943−5945. (b) Wang, S.; Zuo, J. L.; Zhou, H. C.; Song, Y.; Gao, S.; You, X. Z. *Eur. J. Inorg. Chem.* **2004**, 3681−3687. (c) Kim, J.; Han, S.; Pokhodnya, K. I.; Migliori, J. M.; Miller, J. S. *Inorg. Chem*. **2005**, *44*, 6983−6988.

(17) (a) Klausmeyer, K. K.; Rauchfuss, T. B.; Wilson, S. R. *Angew. Chem., Int. Ed*. **1998**, *37*, 1694−1696. (b) Klausmeyer, K. K.; Wilson, S. R.; Rauchfuss, T. B. *J. Am. Chem. Soc*. **1999**, *121*, 2705−2711. (c) Contakes, S. M.; Klausmeyer, K. K.; Rauchfuss, T. B. *Inorg. Chem*. **2000**, *39*, 2069−2075. (d) Darensbourg, D. J.; Lee, W. Z.; Adams, M. J.; Yarbrough, J. C. *Eur. J. Inorg. Chem*. **2001**, 2811−2822.

(18) (a) Oshio, H.; Yamamoto, M.; Ito, T. *Inorg. Chem*. **2002**, *41*, 5817−5820. (b) Oshio, H.; Tamada, O.; Onodera, H.; Ito, T.; Ikoma, T.; Tero-Kubota, S. *Inorg. Chem*. **1999**, *38*, 5686−5689. (c) Oshio, H.; Onodera, H.; Tamada, O.; Mizutani, H.; Hikichi, T.; Ito, T. *Chem.*−*Eur. J*. **2000**, *6*, 2523−2530. (d) Toma, L.; Lescouëzec, R.; Vaissermann, J.; Herson, P.; Marvaud, V.; Lloret, F.; Julve, M. *New J. Chem.* **2005**, *29*, 210−219.

(19) Lescouëzec, R.; Vaissermann, J.; Toma, L. M.; Carrasco, R.; Lloret, F.; Julve, M. *Inorg. Chem*. **2004**, *43*, 2234−2236.

$(CH_3OH)_2(H_2O)_2]\cdot 2H_2O$ (**4**). Interestingly, complex **3** is an unexpected 1D chiral helical chain exhibiting ferromagnetic coupling between Cu^{II} and Fe^{III} ions.

Experimental Section

Materials and Physical Measurements. All chemicals were reagent grade and were used as received. 1,3,5-Tris(2-pyridyl)-triazine was purchased form the Aldrich Chemical Co. Hbpca and $[Fe(bpca)_2]\cdot H_2O$ were prepared according to literature methods.[20,22b] Elemental analyses for C, H, and N were performed on a Perkin-Elmer 240C analyzer. Infrared spectra were recorded on a Vector22 Bruker spectrophotometer with KBr pellets in the 400−4000 cm^{-1} region. The UV−vis absorption spectra were recorded on a Shimadzu UV-3100 spectrometer. The circular dichroism spectra were recorded on a JASCO J-810 spectropolarimeter with KBr pellets. The second-order nonlinear optical effect was determined on a LAB130 Pulsed Nd:YAG laser. The magnetic susceptibility measurements of the polycrystalline samples were measured over the temperature range of 1.8−300 K with a Quantum Design MPMS-XL7 SQUID magnetometer using an applied magnetic field from 100 to 2000 Oe. Field dependences of magnetization were measured using a flux magnetometer in an applied field up to 70 kOe generated by a conventional pulsed technique.

Caution: The cyanides are very toxic and should be handled in small quantities and with great caution.

Preparation of $(Bu_4N)[Fe(bpca)(CN)_3]\cdot H_2O$ (1). A mixture of $[Fe(bpca)_2]\cdot H_2O$ (1.97 g, 3.75 mmol) and KCN (0.98 g, 15 mmol) in 50 mL of 2-propanol was heated at 80 °C for 18 h under continuous stirring. The resulting mixture was cooled to room temperature, and the solvent was removed under reduced pressure. The residue was dissolved in 120 mL of 80 °C hot water, the small fraction of insoluble material being removed by filtration. Twenty milliliters of 30% H_2O_2 (excess) was added successively to the filtrate with continuous stirring until the color of the solution changed from black-green to brown-yellow. Solid $(Bu_4N)Cl$ (2.1 g, 7.5 mmol) was added to the above solution to cause the precipitation of a yellow crystalline solid. The yellow crystalline product was filtered, washed with water, and dried under vacuum at room temperature. Yield: 71%. Anal. Calcd for $C_{31}H_{46}FeN_7O_3$: C, 59.94; H, 7.41; N, 15.79. Found: C, 59.78; H, 7.10; N, 15.77. IR (KBr, cm^{-1}): 2122 (ν_{-CN}).

$[(bpca)_2Fe^{III}_2(CN)_6Cu(H_2O)_2\cdot 1.5H_2O]_n$ (2). Two milliliters of an aqueous solution of $Cu(SiF_6)_2\cdot 4H_2O$ (18.2 mg, 0.06 mmol) was added to the solution of $[Bu_4N][Fe(bpca)(CN)_3]\cdot H_2O$ (60.5 mg, 0.1 mmol) in 30 mL of methanol and water (v/v = 4:1). Slow evaporation of the resulting solution in air yielded brown-yellow crystals after 3 days. Yield: 63%. Anal. Calcd for $C_{60}H_{46}Cu_2Fe_4N_{24}O_{15}$: C, 42.51; H, 2.72; N, 19.84. Found: C, 42.45; H, 2.57; N, 19.68. IR (KBr, cm^{-1}): 2136 (ν_{-CN}), 2168 ($\nu_{\mu-CN}$).

$[(bpca)Fe^{III}(CN)_3Cu(bpca)(H_2O)\cdot H_2O]_n$ (3). Solid $Cu(ClO_4)_2\cdot 6H_2O$ (18.5 mg, 0.05 mmol) and Hbpca (11.4 mg, 0.05 mmol) were mixed in 10 mL of MeCN/H_2O (v/v = 4:1). Then an acetonitrile solution (5 mL) of $(Bu_4N)[(bpca)Fe(CN)_3]\cdot H_2O$ (30.2 mg, 0.05 mmol) was added to the solution. Slow evaporation of the resulting dark green solution at room temperature yielded dark green crystals of **3** suitable for X-ray diffraction. Yield: 76%. Anal. Calcd for $C_{27}H_{20}CuFeN_9O_6$: C, 47.28; H, 2.94; N, 18.38; Found: C, 47.02; H, 3.16; N, 18.36. IR data (KBr, ν_{max}, cm^{-1}): 2125 (ν_{-CN}), 2177 ($\nu_{\mu-CN}$).

$[(bpca)_2Fe^{III}_2(CN)_6Mn(CH_3OH)_2(H_2O)_2]\cdot 2H_2O$ (4). Five milliliters of an aqueous solution of $MnCl_2\cdot 4H_2O$ (10 mg, 0.05 mmol) was added to a solution of $[Bu_4N][Fe(bpca)(CN)_3]\cdot H_2O$ (60.5 mg, 0.1 mmol) in 10 mL of methanol and water (v/v = 4:1). Slow evaporation of the resulting solution at room temperature in air yielded orange-yellow crystals after 3 days, which were collected by filtration. Yield: 65%. Anal. Calcd for $C_{32}H_{32}Fe_2MnN_{12}O_{10}$: C, 42.14; H, 3.51; N, 18.43. Found: C, 41.85; H, 3.45; N, 18.10. IR (KBr, cm^{-1}): 2132 (ν_{-CN}), 2155 ($\nu_{\mu-CN}$).

X-ray Crystallography. The crystal structures of complexes **2**, **3**, and **4** were determined on a Siemens (Bruker) SMART CCD diffractometer using monochromated Mo Kα radiation ($\lambda = 0.71073$ Å). Cell parameters were retrieved using SMART software and refined using SAINT on all observed reflections. Data were collected using the following strategy: 606 frames of 0.3° in ω with $\phi = 0°$, 435 frames of 0.3° in ω with $\phi = 90°$, and 235 frames of 0.3° in ω with $\phi = 180°$. An additional 50 frames of 0.3° in ω with $\phi = 0°$ were collected to allow for decay correction. The highly redundant data sets were reduced using SAINT and corrected for Lorentz and polarization effects. Absorption corrections were applied using SADABS (supplied by Bruker). Structures were solved by direct methods using the program SHELXL-97. The positions of the metal atoms and their first coordination spheres were located from direct-method *E* maps; other non-hydrogen atoms were found using alternating difference Fourier syntheses and least-squares refinement cycles and, during the final cycles, were refined anisotropically. Hydrogen atoms were placed in calculated position and refined as riding atoms with a uniform value of U_{iso}. Final crystallographic data and values of R_1 and R_2 are listed in Table 1. The Flack value for complex **3** is −0.007(9).

Table 1. Crystallographic Data for Complexes **2**, **3** and **4**

	2	**3**	**4**
empirical formula	$C_{60}H_{46}Cu_2Fe_4N_{24}O_{15}$	$C_{27}H_{20}CuFeN_9O_6$	$C_{48}H_{48}Fe_3Mn_{1.5}N_{18}O_{15}$
fw	1693.69	685.91	1367.00
cryst syst	monoclinic	orthorhombic	monoclinic
space group	$P2_1/c$	$P2_12_12_1$	$C2/c$
a (Å)	16.097(3)	10.6602(10)	15.5338(4)
b (Å)	15.619(3)	11.9053(13)	26.2245(8)
c (Å)	14.524(2)	22.724(2)	29.4515(9)
α (deg)	90	90	90
β (deg)	112.267(3)	90	102.472(2)
γ (deg)	90	90	90
V (Å^3)	3379.3(9)	2884.0(5)	11714.4(6)
Z	2	4	8
ρ_{calcd} (g cm^{-3})	1.665	1.580	1.550
T (K)	293(2)	293(2)	293(2)
μ (mm^{-1})	1.539	1.299	1.122
F(000)	1712	1392	5580
index ranges	$-15 \le h \le 19$ $-19 \le k \le 19$ $-17 \le l \le 11$	$-14 \le h \le 5$ $-15 \le k \le 14$ $-30 \le l \le 20$	$-19 \le h \le 19$ $-29 \le k \le 32$ $-36 \le l \le 36$
data/restraints/params	6620/0/479	6761/0/397	11479/0/775
GOF (F^2)	1.115	1.012	1.149
R_1,[a] R_2[b] ($I > 2\sigma(I)$)	0.0455, 0.0956	0.0311, 0.0678	0.0506, 0.0820
R_1,[a] R_2[b] (all data)	0.0645, 0.1008	0.0424, 0.0703	0.0725, 0.0853

[a] $R_1 = \sum||F_o| - |F_c||/\sum F_o|$. [b] $R_2 = [\sum w(F_o^2 - F_c^2)^2/\sum w(F_o^2)]^{1/2}$.

Results and Discussion

Syntheses. The anionic precursor $[Fe(bpca)(CN)_3]^-$ (**1**) was chosen as the building block for the preparation of

(20) Kamiyama, A.; Noguchi, T.; Kajiwara, T.; Ito, T. *Inorg. Chem.* **2002**, *41*, 507−512.
(21) Kurtz, S. K.; Perry, T. T. *J. Appl. Phys.* **1968**, *39*, 3798−3813.
(22) (a) Kajiwara, T.; Ito, T. *Acta Crystallogr.* **2000**, *C56*, 22−23. (b) Wocadlo, S.; Massa, W.; Folgado, J. V. *Inorg. Chim. Acta* **1993**, *207*, 199−206.

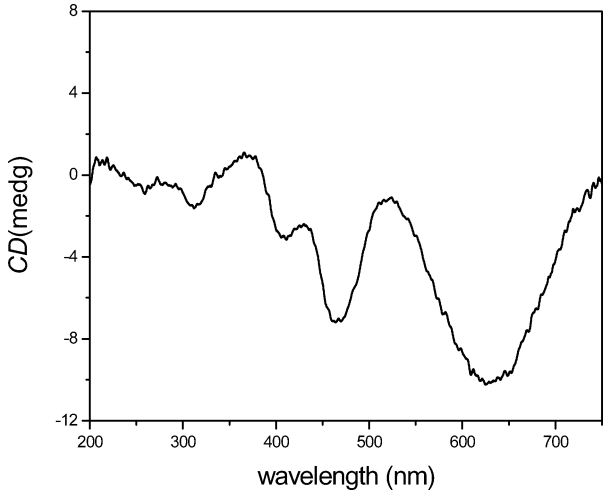

Figure 1. Circular dichroism spectrum of complex **3** in KBr pellets.

cyano-bridged heterobimetallic coordination polymers and multinuclear clusters. The preparation of the tetraphenylphosphonium salt of **1** has been reported.[19] In this paper, we prepared the tetrabutylammonium salt of **1**, and it was isolated as a yellow crystalline solid in a 71% yield. It is soluble in common organic solvents such as acetonitrile, methanol, and acetone.

The reaction of $(Bu_4N)[Fe(bpca)(CN)_3]$ (**1**) and $CuSiF_6 \cdot 4H_2O$ in methanol and water yields a cyano-bridged one-dimensional heterobimetallic complex, $[(bpca)_2Fe^{III}{}_2(CN)_6Cu(H_2O)_2 \cdot 1.5H_2O]_n$ (**2**). The trinuclear complex, $[(bpca)_2Fe^{III}{}_2(CN)_6Mn(CH_3OH)_2(H_2O)_2] \cdot 2H_2O$ (**4**), is synthesized from the reaction of **1** and $MnCl_2 \cdot 4H_2O$ in methanol and water. Suitable crystals for structural determination were obtained by the slow evaporation of the dilute preparative solution.

The reaction of $(Bu_4N)[(bpca)Fe(CN)_3] \cdot H_2O$, $Cu(ClO_4)_2 \cdot 6H_2O$ and Hbpca in a mixture of acetonitrile and water yielded an unexpected chiral heterobimetallic helical chain complex, $[(bpca)Fe^{III}(CN)_3Cu(bpca)(H_2O) \cdot H_2O]_n$ **(3)**. To our surprise, the synthesis did not involve any chiral reactant, solvent, or other auxiliary agent, but the resultant crystals were not racemic as shown by the observation of strong signals in circular dichroism (CD) spectrum (Figure 1). We have made independent preparations using different reaction volumes and amounts, and we randomly picked out more than forty pieces of crystal from the resultant crystals to measure the CD spectra for each batch reaction. The CD spectra of all measured crystals exhibited essentially the same Cotton effect. We could not find a reasonable explanation for the enantiomeric excess phenomenon.

Spectroscopic Studies. Only one C≡N stretching vibration (2122 cm^{-1}) was observed in the IR spectrum for complex **1**, which is in accordance with the presence of the same terminal cyanide groups. Two sharp peaks of medium intensity (2136 and 2168 cm^{-1} for **2**, 2125 and 2177 cm^{-1} for **3**, and 2132 and 2155 cm^{-1} for **4**) in the C≡N stretching region of the IR spectra were observed: these peaks are consistent with the presence of both terminal and bridging cyanide groups.

According to the principle proposed by Kurtz and Perry,[21] we estimated the second-order nonlinear optical effect of complex **3**, and it shows an SHG efficiency with a value of 0.4 times that of urea. The circular dichroism (CD) spectrum of complex **3** in KBr pellets was measured to confirm the optical activity of this compound. The CD spectrum of complex **3** exhibits a negative Cotton effect at $\lambda_{max} = 450$ and 625 nm, which can be assigned to the charge-transfer and d−d transitions of the UV−vis absorption spectra, respectively (Figure 1). However, the starting materials and solvents, as well as the mother liquor, were not found to have any optical rotation.

Table 2. Selected Bond Lengths (Å) and Angles (deg) for Complex **2**[a]

Cu(1)−N(11)#1	1.967(2)	Fe(2)−N(5)	1.896(3)
Cu(1)−N(12)#2	1.967(2)	Fe(2)−N(4)	1.936(2)
Cu(1)−N(7)	2.006(2)	Fe(2)−C(17)	1.942(3)
Cu(1)−N(8)	2.012(2)	Fe(2)−C(18)	1.949(3)
Cu(1)−O(5)	2.267(2)	Fe(2)−C(16)	1.988(3)
Fe(1)−N(2)	1.888(2)	Fe(2)−N(6)	2.007(2)
Fe(1)−C(13)	1.940(3)	C(13)−N(10)	1.116(4)
Fe(1)−C(14)	1.959(3)	C(14)−N(8)	1.136(4)
Fe(1)−N(3)	1.962(2)	C(15)−N(11)	1.102(4)
Fe(1)−C(15)	1.965(3)	C(16)−N(7)	1.131(4)
Fe(1)−N(1)	1.966(3)		

N(11)#1−Cu(1)−N(7)	87.78(11)	N(7)−Cu(1)−O(5)	91.01(10)
N(12)#2−Cu(1)−N(7)	93.13(11)	N(8)−Cu(1)−O(5)	89.35(10)
N(11)#1−Cu(1)−N(8)	92.46(11)	N(7)−Cu(1)−N(8)	179.55(11)
N(12)#2−Cu(1)−N(8)	86.57(10)	N(11)#1−Cu(1)−N(12)#2	171.20(12)
N(11)#1−Cu(1)−O(5)	95.82(10)	C(16)−N(7)−Cu(1)	171.4(3)
N(12)#2−Cu(1)−O(5)	92.92(11)	C(14)−N(8)−Cu(1)	174.8(2)

[a] Symmetry transformations used to generate equivalent atoms: #1 x, $-y + 3/2$, $z + 1/2$; #2 x, $-y + 3/2$, $z - 1/2$.

Table 3. Selected Bond Lengths (Å) and Angles (deg) for Complex **3**

Cu(1)−N(6)	1.953(2)	Fe(1)−C(14)	1.958(3)
Cu(1)−N(7)	2.017(2)	Fe(1)−C(15)	1.941(2)
Cu(1)−N(8)	1.941(2)	C(15)−N(6)	1.144(3)
Cu(1)−N(9)	2.015(2)	C(13)−N(4)	1.138(3)
Cu(1)−O(6)	2.4308(19)	C(14)−N(5)	1.140(3)
Fe(1)−N(1)	1.971(2)	N(2)−C(6)	1.396(3)
Fe(1)−N(2)	1.8862(19)	N(2)−C(7)	1.372(3)
Fe(1)−N(3)	1.964(2)	C(6)−O(1)	1.208(3)
Fe(1)−C(13)	1.971(3)	C(7)−O(2)	1.219(3)

O(6)−Cu(1)−N(6)	84.11(8)	Cu(1)−N(6)−C(15)	169.5(2)
O(6)−Cu(1)−N(7)	100.19(8)	N(6)−C(15)−Fe(1)	176.3(2)
O(6)−Cu(1)−N(8)	93.98(8)	N(4) −C(13)−Fe(1)	177.8(2)
O(6)−Cu(1)−N(9)	91.89(8)	N(5) −C(14)−Fe(1)	176.8(2)
N(6)−Cu(1)−N(8)	178.05(9)	C(15) −Fe(1)−N(2)	177.04(9)
N(7)−Cu(1)−N(9)	160.16(8)	N(1) −Fe(1)−N(3)	165.99(8)

Crystal Structures. Selected bond lengths and angles for complexes **2**, **3**, and **4** are collected in Tables 2−4.

The ORTEP drawing for complex **2**, $[(bpca)_2Fe^{III}{}_2(CN)_6Cu(H_2O)_2 \cdot 1.5H_2O]_n$, is depicted in Figure 2. It consists of $Fe_2(CN)_4Cu_2$ squares and forms a neutral one-dimensional bimetallic chain (Figure 3). Within the chain, the central Cu^{II} ion is six-coordinated as an elongated distorted octahedron, CuN_4O_2. The equatorial plane is formed by four nitrogen atoms from four cyanide groups of $[Fe(bpca)(CN)_3]^-$ with the average bond lengths of Cu−N being 1.988(2) Å. The apical positions are occupied by two oxygen atoms (O(5) and O(6)) of two water molecules with the different bond lengths of 2.267(2) (Cu(1)−O(5)) and 2.575(2) Å (Cu(1)−O(6)). In the equatorial plane, the bond angles of N(11)#1−Cu(1)−N(8), N(12)#2−Cu(1)−N(8), N(11)#1−Cu(1)−N(7), and N(12)#2−Cu(1)−N(7) are 92.46(11), 86.57(10), 87.78(11), and 93.13(11)°, respectively: they deviate slightly from

Table 4. Selected Bond Lengths (Å) and Angles (deg) for Complex **4**[a]

Mn(1)−N(6)	2.188(3)	Mn(2)−O(13)#1	2.200(2)
Mn(1)−N(12)	2.203(3)	Fe(1)−N(1)	1.971(3)
Mn(1)−O(5)	2.157(2)	Fe(1)−N(2)	1.904(3)
Mn(1)−O(6)	2.218(2)	Fe(1)−N(3)	1.956(3)
Mn(1)−O(7)	2.189(2)	Fe(1)−C(13)	1.944(3)
Mn(1)−O(8)	2.205(2)	Fe(1)−C(14)	1.946(3)
Mn(2)−N(17)	2.190(3)	Fe(1)−C(15)	1.960(3)
Mn(2)−N(17)#1	2.190(3)	C(13)−N(4)	1.157(4)
Mn(2)−O(11)	2.211(3)	C(14)−N(5)	1.145(4)
Mn(2)−O(12)	2.140(3)	C(15)−N(6)	1.145(4)
Mn(2)−O(13)	2.200(2)	C(30)−N(12)	1.128(4)
N(6)−Mn(1)−O(5)	89.34(10)	N(17)−Mn(2)−O(12)	92.35(7)
N(6)−Mn(1)−O(6)	91.52(9)	N(17)−Mn(2)−O(13)	92.92(10)
N(6)−Mn(1)−O(7)	97.80(9)	N(17)−Mn(2)−O(13)#1	86.73(11)
N(6)−Mn(1)−O(8)	83.07(10)	O(11)−Mn(2)−O(13)#1	85.07(6)
O(5)−Mn(1)−O(6)	90.66(9)	O(12)−Mn(2)−O(13)	94.93(6)
O(7)−Mn(1)−O(8)	87.24(9)	O(13)−Mn(2)−O(13)#1	170.14(12)
O(5)−Mn(1)−O(8)	170.58(9)	O(11)−Mn(2)−O(12)	180.0
O(6)−Mn(1)−O(7)	170.60(8)	Mn(2)−N(17)−C(47)	161.8(3)
Mn(1)−N(6)−C(15)	171.0(3)	N(17)−Mn(2)−N(17)#1	175.21(16)
Mn(1)−N(12)−C(30)	168.3(3)	N(6)−C(15)−Fe(1)	178.1(3)
N(6)−Mn(1)−N(12)	172.05(11)	N(4)−C(13)−Fe(1)	174.8(3)
N(17)−Mn(2)−O(11)	87.65(7)		

[a] Symmetry transformations used to generate equivalent atoms: #1 $-x$, y, $-z + 1/2$.

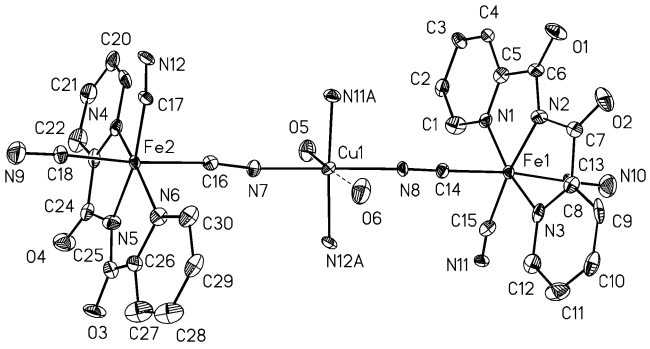

Figure 2. Structure of segments of the 1D chain complex **2** (thermal ellipsoids are shown at the 30% probability level). Hydrogen atoms and noncoordinated crystalline water molecules are omitted for clarity.

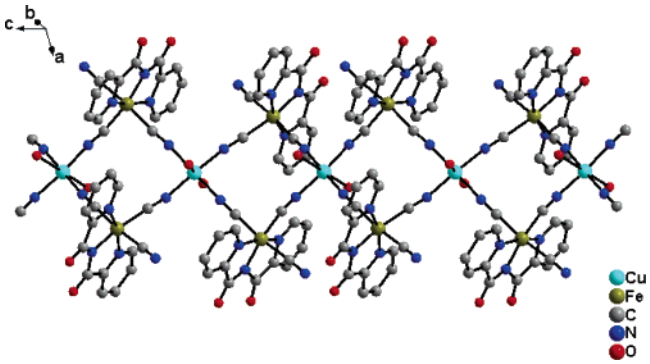

Figure 3. Perspective view of the 1D square-chain configuration with the atomic labeling scheme for complex **2**.

90°. In $[Fe(bpca)(CN)_3]^-$, three cyanide ligands in a mer arrangement and the tridentate N-donor ligand, bis(2-pyridylcarbomyl)amidate, form a distorted octahedral environment around the iron(III) ion. The Fe(1)−C(cyano) bond lengths (1.940(3)−1.965(3) Å) are in good agreement with those observed in another low-spin iron(III) cyanide complex.[5a] Each $[Fe(bpca)(CN)_3]^-$ unit provides two cyanide groups (one is in the equatorial plane and the other is in the axial

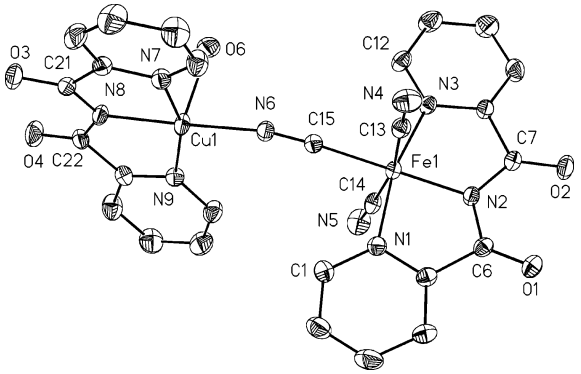

Figure 4. Molecular structure and labeling scheme of complex **3** (thermal ellipsoids drawn at the 50% probability level). Water molecules and hydrogen atoms are omitted for clarity.

direction) to coordinate with neighboring Cu^{II} atoms and leaves one cyanide group free, which is consistent with the occurrence of both bridging and free terminal cyanide groups observed in the IR spectrum. The shortest intrachain Cu···Cu, Cu···Fe, and Fe···Fe distances are 7.263, 4.964, and 6.702 Å, respectively. Each chain interacts with other adjacent chains by hydrogen bonding (for example, O(5)−H(5A)···O(4) = 2.841(4) Å, O(2)−H(6A)···O(6) = 2.738(7) Å) and other short intermolecular distance interactions (Figure S1). The shortest interchain Cu···Cu, Fe···Fe, and Cu···Fe separations are 11.214, 7.205, and 7.938 Å, respectively.

Complex **3** crystallizes in the chiral space group $P2_12_12_1$ with a right-handed 1D helical chain structure. The 1D helical chain consists of the asymmetric unit of $[(bpca)Fe(CN)_3Cu(bpca)(H_2O)]$ shown in Figure 4, in which the $[(bpca)Fe(CN)_3Cu(bpca)(H_2O)]$ unit propagates along the *a* axis by the bridging cyanide group (Figure 5). Within the chain, there are two kinds of inequivalent cyanide-bridged groups, the shorter one (Cu(1)−N(6) = 1.953(2) Å) and the longer one (Cu(1)−N(5)#1 = 2.632 Å; the symmetric operation is $1/2 + x$, $3/2 - y$, $2 - z$) are alternatively arranged. The N(7)−C(21)−N(8)−C(22)−N(9)−Cu(1) plane is almost perpendicular to the N(1)−C(6)−N(2)−C(7)−N(3)−Fe(1) plane with a dihedral angle of 84.4°. Each $[(bpca)Cu(H_2O)]^+$ is linked to two $[(bpca)Fe(CN)_3]^-$ ions by cis-position cyanide groups to form the 1D alternating helical chain (Figure 5). The Cu^{II} is six-coordinated in an elongated distorted octahedral environment; four nitrogen atoms from a bpca ligand and a cyanide group of $[(bpca)Fe(CN)_3]^-$ form the equatorial plane with bond distances of 1.941(2)−2.017(2) Å, and the stretched axial positions were occupied by the one oxygen atom of H_2O (Cu(1)−O(6) = 2.4308(19) Å) and a cyanide group nitrogen atom of $[(bpca)Fe(CN)_3]^-$ (Cu(1)−N(5)#1 = 2.632 Å). The Fe^{III} has a distorted octahedral geometry, completed by three nitrogen atoms from a bpca ligand and three carbon atoms from the cyanide groups. The Fe(1)−N(bpca) bond lengths (1.8862(19)−1.971(2) Å) are considerably shorter than those found in the high-spin iron(III) complex.[22] The Fe(1)−C(cyano) bond lengths (1.941(2)−1.971(3) Å) are in good agreement with those observed in the other low-spin iron(III) cyanide complex. Each chain interacts with other adjacent chains by hydrogen bonds and

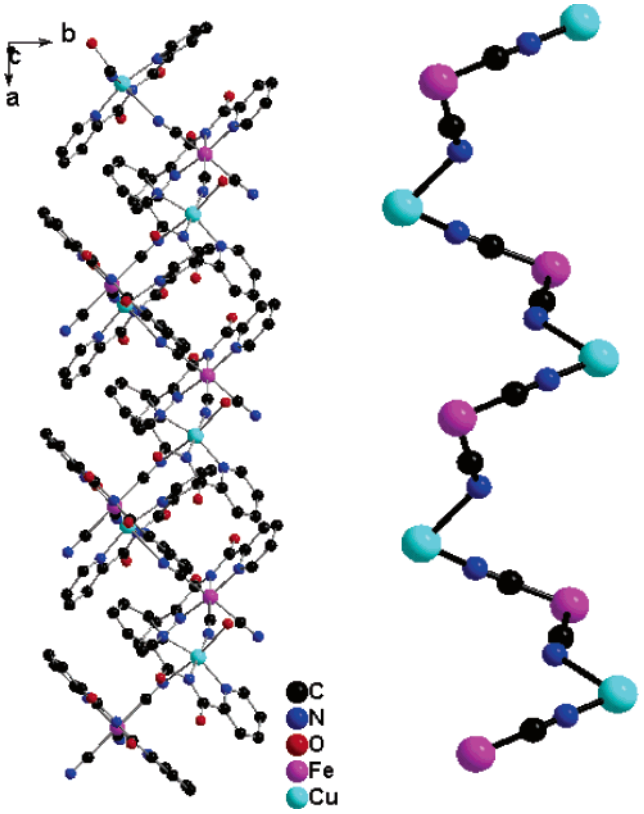

Figure 5. View of the 1D chiral right-handed helical chain of complex **3** along the *a* axis.

the shortest N···O interaction to form the chiral crystal (Figure S2). The shorter intrachain Fe···Cu distances are 5.007(2) and 5.144(2) Å, and the shortest interchain Fe···Fe, Cu···Cu, and Fe···Cu distances are 8.190(2), 7.887(2), and 8.219(2) Å, respectively.

The ORTEP drawing for complex **4** is depicted in Figure 6a and b. In this trinuclear cluster, the $[Fe(bpca)(CN)_3]^-$ unit is coordinated to the central $[Mn(CH_3OH)_2(H_2O)_2]^{2+}$ core as a monodentate ligand through one cyanide group. The manganese atom is six-coordinated in a slightly distorted octahedral geometry. Four oxygen atoms from the two methanol and two water molecules form the equatorial plane. Interestingly, in the two independent trinuclear clusters of the same asymmetric unit, there are two different coordination modes (cis and trans) for the two methanol or two water molecules coordinated to the central Mn(II) ion. The Mn(1)−O bond lengths in the cis fragments (2.157(2)−2.218(2) Å) are slightly longer than those in trans fragments (Mn(2)−O = 2.140(3)−2.211(3) Å). The bond angles of N(6)−Mn(1)−O(5), N(6)−Mn(1)−O(8), N(17)−Mn(2)−O(11), and N(17)−Mn(2)−O(13) are 89.34(10), 83.07(10), 87.65(7), and 92.92(10)°, respectively, which deviate significantly from 90°. Two cyanide nitrogen atoms occupy the axial positions with bond lengths of 2.188(3) (Mn(1)−N(6)), 2.203(3) (Mn(1)−N(12)), and 2.190(3) Å (Mn(2)−N(17) and Mn(2)−N(17)#1). The bond angles of Mn(1)−N(6)−C(15), Mn(1)−N(12)−C(30), and Mn(2)−N(17)−C(47) are 170.9(3), 168.3(3), and 161.8(3)°, respectively, which deviate significantly from 180°. Noncoordinated water molecules are inserted into the crystal spaces. The packing diagram for

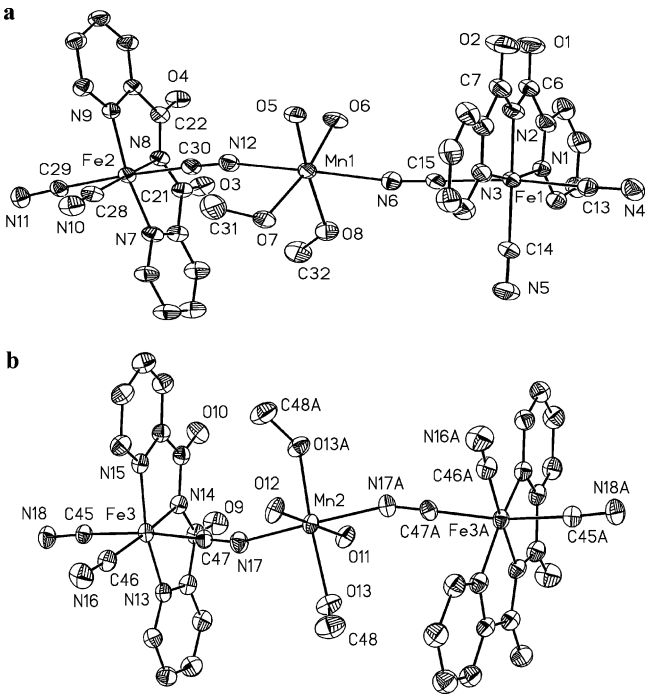

Figure 6. Structure of the trinuclear complex **4** (a and b) (thermal ellipsoids are shown at the 50% probability level). Hydrogen atoms and noncoordinated crystalline water molecules are omitted for clarity.

complex **4** is shown in Figure S3. There are hydrogen bonds and short distance intermolecular interactions between the molecules in the crystal. Hydrogen bonding interactions between the molecules occur at N(5)−H(7)···O(7) (2.829(5) Å), N(10)−H(12B)···O(12) and N(10)−H(12C)···O(12) (2.813(4) Å), and N(11)−H(14B)···O(14) (2.825(4) Å). The shortest intramolecular Fe···Mn and Fe···Fe separations are 5.223 and 10.416 Å, respectively, and the shortest intermolecular Fe···Fe, Mn···Fe, and Mn···Mn distances are 8.101, 7.391, and 8.019 Å, respectively.

Magnetic Properties. Magnetic measurements were performed on polycrystalline samples of complexes **1**−**4**. For complex **1**, the $\chi_M T$ values are constant at 0.44 emu K mol^{-1} over the whole temperature range under an applied field of 2 kOe (Figure S4), indicating the paramagnetic properties on this complex with the low-spin Fe^{III} state, and the *g* value obtained is 2.17. At the same field, the variable-temperature magnetic properties from 300 to 1.8 K were measured for complex **2** as shown in Figure 7. At room temperature, $\chi_M T$ is 1.28 emu K mol^{-1}, which is close to the theoretical value, 1.29 emu K mol^{-1}, based on the $CuFe_2$ unit ($S_{Cu} = S_{Fe} = 1/2$, $g_{Fe} = 2.17$, and assuming $g_{Cu} = 2.1$) without any interaction between ions. As the temperature decreases, $\chi_M T$ gradually increases and reaches 2.26 emu K mol^{-1} at 30 K, and then it abruptly increases reaching 9.70 emu K mol^{-1} at 4 K, indicating the ferromagnetic coupling between the Cu^{II} and Fe^{III} ions in this system. Below 4 K, $\chi_M T$ sharply drops to 5.10 emu K mol^{-1} at 1.8 K. Further evidence of ferromagnetic coupling between the metal ions comes from the field dependence of magnetization measurements at 1.8 K (Figure 8). The magnetization increases with increasing field and is saturated above 2 T. The saturating value of 3.25 $N\beta$ mol^{-1} at 7 T corresponds to the expected spontaneous

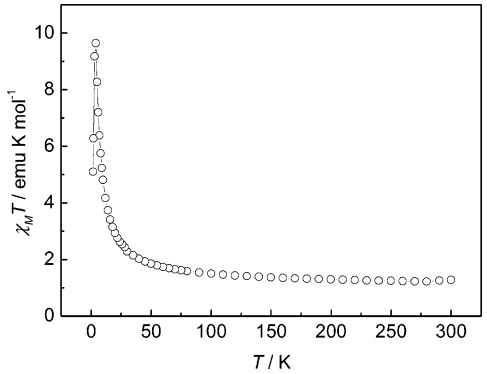

Figure 7. Temperature dependence of magnetic susceptibility in the form of $\chi_M T$ vs T at 2 kOe for complex **2**. The solid line is a guide for eyes.

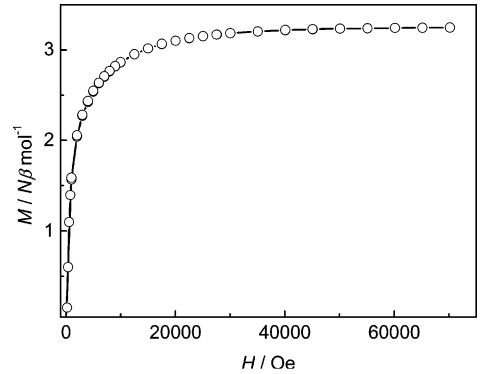

Figure 8. Field dependence of magnetization at 1.8 K for complex **2**. The solid line is a guide for eyes.

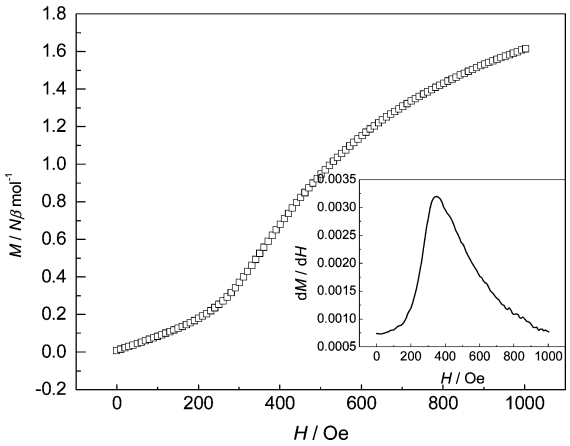

Figure 9. Low-field magnetization measurements for complex **2**.

magnetization of 3.22 $N\beta$ mol^{-1} for the parallel ordering unpaired electrons of the $CuFe_2$ unit ($S_{Cu} = S_{Fe} = 1/2$, $g_{Fe} = 2.17$, and assuming $g_{Cu} = 2.1$). In the low-field magnetization measurements at 1.8 K, an S-shaped curve was observed as shown in Figure 9, which is typical of metamagnetic behavior. Below about 250 Oe, complex **2** shows antiferromagnetic properties. As the field increases, the antiparallel unpaired electrons are driven by the applied field and change into a spin-canting state. At higher fields, all unpaired electrons become parallel to each other and reach ferromagnetic ordering. The metamagentic phenomenon of complex **2** is also confirmed by the AC magnetic measurements. When $H_{dc} = 0$, a peak was observed at 2.2 K in the in-phase variable-temperature magnetization, m', but the out-of-phase

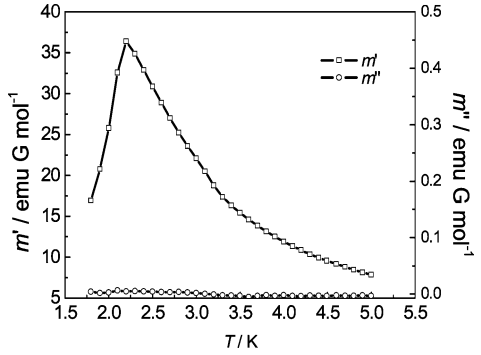

Figure 10. AC magnetization measurements for complex **2** at $H_{ac} = 1$ Oe, $H_{dc} = 0$, and $f = 10$ Hz.

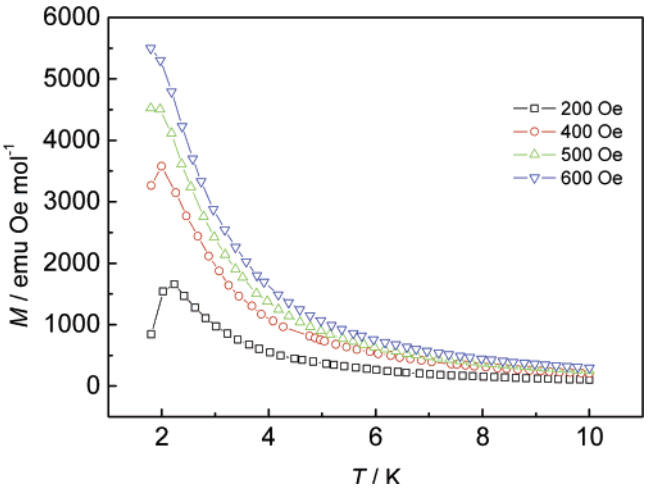

Figure 11. Low-temperature magnetization measurements around the critical field for complex **2**.

variable-temperature magnetization, m'', is zero, indicating antiferromagnetic ordering, T_N, at this temperature (Figure 10). When the applied field is high, 2 and 4 kOe, both in-phase and out-of-phase peaks were observed in the AC magnetic measurements (Figure S6), indicating field-induced ferromagnetic ordering, T_c, in complex **2**. Equally, the maximum in the M versus T curve at low fields supports the metamagentic behavior in complex **2** (Figure 11). At 200 Oe, a sharp peak was observed at 2.2 K because the antiferromagnetic interchain interactions through a network of hydrogen bonds lead to an antiferromagnetic ordering. The maximum broadens and shifts to lower temperature as the magnetic field increases, and it finally disappears for $H \geq 500$ Oe. This behavior shows the existence of a field-induced transition from an antiferromagnetic ground state to a ferromagnetic state. From the variable-field (Figure 9) and variable-temperature magnetization measurements at low fields (Figure 11), the critical field may be estimated to be about 250 Oe, and the spin-canting state is in the range of 250−500 Oe. According to the structure of complex **2** and the saturation value at 7 T, the metamagnetic behavior can be attributed to the field-induced interchain long-range magnetic ordering with intrachain ferromagnetic coupling between Cu^{II} and Fe^{III} ions. It is noteworthy that this critical field is very low, which indicates that the interchain interaction is very weak. A similar 1D square-chain compound with a slightly modified capping ligand, $[(Tp)_2Fe^{III}{}_2$-

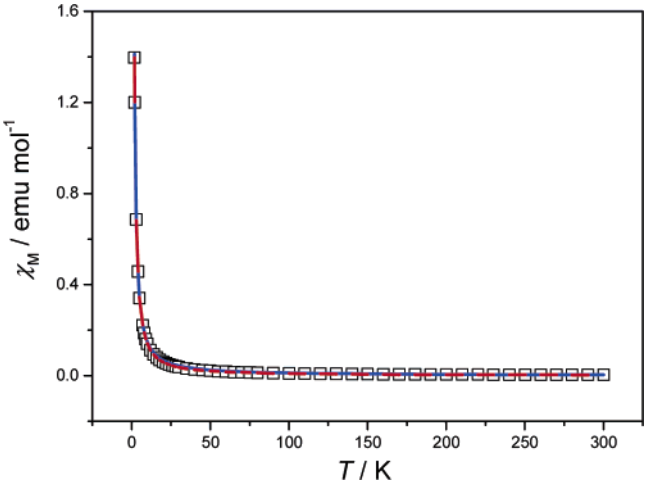

Figure 12. Temperature dependence of χ_M for complex **3**. The solid line corresponds to the best-fit curves (blue for the dimer model and red for the chain model).

$(CN)_6Cu(CH_3OH)\cdot 2CH_3OH]_n$, shows single-chain magnet (SCM) behavior.[5c]

In the structure of complex **2**, the Cu^{II} ion is located at the center of a distorted elongated octahedron environment attributed to the Jahn−Teller effect, so the magnetic orbital is defined on $d_{x^2-y^2}$ in the plane of $Cu(NC)_4$. For the low spin $[Fe(bpca)(CN)_3]^-$ unit, the magnetic orbital is d_{xy} in the plane of the three cyanide groups (defined by N5−Fe−$(CN)_3$, Figure 2).[19] Thus, the magnetic orbital of the Fe^{III} ion is exactly orthogonal to those of two neighboring Cu^{II} ions in both the orbital orientation and orbital symmetry, further leading to the intrachain ferromagnetic interaction between the Cu^{II} and Fe^{III} ions. From the magnetic measuring results mentioned above, the coupling interaction between the Cu^{II} and Fe^{III} ions should be weak. Unfortunately, the lack of an appropriate model for investigating the magnetic properties of the bimetallic ladderlike chain impedes the evaluation of the ferromagnetic J value in theory.

The temperature dependence of the χ_M (Figure 12) for complex **3** shows that the change in the value of χ_M is very small from room temperature to 50 K. Below 20 K, the value of χ_M increases rapidly as the temperature decreases, reaching 1.4 emu mol^{-1} at 1.8 K. Figure 13 shows the temperature dependence of $\chi_M T$; the $\chi_M T$ value gradually increases from 0.91 emu K mol^{-1} at room temperature to 1.21 emu K mol^{-1} at 20 K, and below 20 K, the $\chi_M T$ value increases rapidly as the temperature decreases further, which indicates the presence of ferromagnetic coupling between the cyanide-bridged Cu^{II} and Fe^{III} ions. The field dependence of magnetization (0−70 KOe) measured at 1.8 K shows the saturation of the magnetization (Figure 13, inset) reaching 2.11 $N\beta$ at 70 KOe for a ferromagnetic binuclear copper(II) and low-spin iron(III) system. When a dimer model that takes the interdimer interaction with Hamiltonian $\hat{H} = 2J\hat{S}_1\hat{S}_2$ into account was used here, the best fit by least-squares gives: $g = 2.25(2)$, $J = 8(2)$ cm^{-1}, and $zj' = 0.49(1)$ cm^{-1} with $R = \sum[(\chi_M T)_{calcd} - (\chi_M T)_{obsd}]^2/\sum(\chi_M T)_{obsd}^2 = 0.004$ as shown in Figure 13. This result indicates that the cyanide ligand mediates the weak ferromagnetic coupling between the Cu^{II} and Fe^{III} ions from the orthogonal magnetic orbitals d_{z^2} of

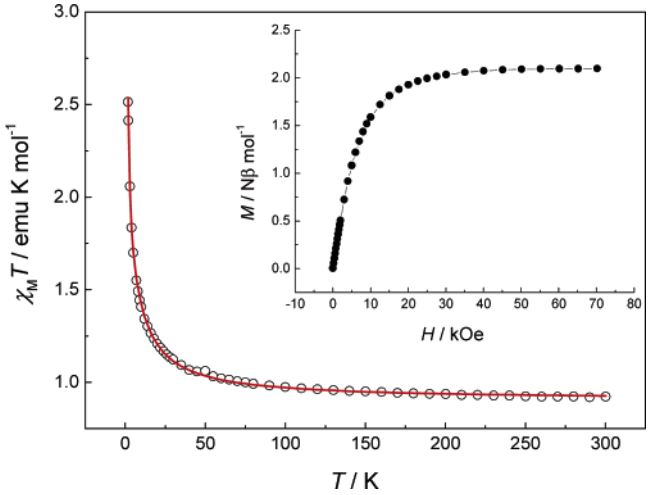

Figure 13. Temperature dependence of $\chi_M T$ for complex **3**. The solid line corresponds to the best-fit curve using the parameters described in the text. The inset shows the magnetization versus the applied magnetic field at 1.8 K.

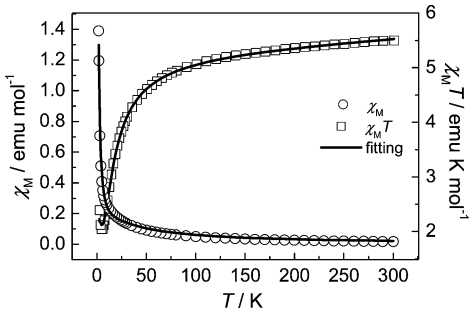

Figure 14. Temperature dependence of magnetic susceptibility in the form of χ_M and $\chi_M T$ vs T at 2 kOe for complex **4**. The solid lines are the fitting from 300 to 1.8 K.

Cu^{II} and d_{xy} of Fe^{III}.[19] However, the large agreement factor, R, suggests that this fitting is rough for complex **3**. According to the structural data, the dimers are linked by a weak contact Cu···N≡C−Fe (Cu(1)−N(5)#1 = 2.632 Å) to form a 1D alternating chain, so the 1D alternating chain model reported by Rojo et al.[23] seems to be more appropriate for the magnetic investigation of complex **3**. For the systems with $S < 5/2$, Kou's[24] treatment was adopted (i.e., the 1D alternating chain can be treated as a uniform CuFe chain with the intradimeric and interdimeic exchange constants (J_d and J_c))

$$\chi_d = \frac{Ng^2\beta^2}{3kT}\frac{6}{3 + \exp(-2J_d/kT)} \quad (1)$$

$$\chi_d = \frac{Ng^2\beta^2}{3kT}S_d(S_d + 1) \quad (2)$$

$$\chi_{chain} = \frac{Ng^2\beta^2}{3kT}\frac{1+u}{1-u}S_d(S_d + 1) \quad (3)$$

where $u = \coth(J_cS_d(S_d + 1)/kT) - kT/J_cS_d(S_d + 1)$.

(23) Cortés, R.; Drillon, M.; Solans, X.; Lezama, L.; Rojo, T. *Inorg. Chem.* **1997**, *36*, 677−683.
(24) Kou, H. Z.; Zhou, B. C.; Liao, D. Z.; Wang, R. J.; Li, Y. *Inorg. Chem.* **2002**, *41*, 6887−6891.

The best-fit parameters for $\chi_M T$ versus T were $J_1 = 7.9(3)$ cm^{-1}, $J_2 = 1.03(2)$ cm^{-1}, and $g = 2.196(3)$ with the final agreement factor $R = 1.2 \times 10^{-4}$. The above fitting results are close to those for the intradimeric coupling between Cu^{II} and Fe^{III} ions, but the chain model is perhaps more reasonable than the dimer model for complex **3**.

Complex **4** shows very different magnetic properties from those of complexes **2** and **3** because of their different molecular and electronic structures. The temperature dependence of susceptibility in the forms of χ_M and $\chi_M T$ versus T at 2 kOe are shown in Figure 14. At room temperature, the $\chi_M T$ value is 5.51 emu K mol^{-1}, which is close to the spin-only value of 5.26 emu K mol^{-1} based on the $MnFe_2$ unit ($S_{Mn} = 5/2$, $S_{Fe} = 1/2$, $g_{Mn} = 2.0$, and $g_{Fe} = 2.17$). As the temperature decreases, $\chi_M T$ gradually decreases reaching a minimum value of 2.05 emu K mol^{-1} at 4 K, corresponding to the antiferromagnetic ground-state spin $S = 3/2$ with $g_{average} = 2.11$ ($g_{average}^2 = 2g_{Fe}^2 + g_{Mn}^2$ and $\chi_M T = 0.125 g_{average}^2 S(S + 1) = 2.09$ emu K mol^{-1}). When the temperature is further lowered, $\chi_M T$ increases, indicating the presence of the ferromagnetic intertrimer interaction in the low temperature region. It is confirmed by the field dependence of magnetization measurements at 1.8 K (Figure 15). The magnetization gradually increases with the applied field and reaches a saturating value of 2.90 $N\beta$ mol^{-1}, which is close to theoretical value of 2.83 $N\beta$ mol^{-1} ($2 \times 5/2 - 2.17 \times 1/2 \times 2$) with antiferromagnetic coupling between the Mn^{II} and Fe^{III} ions. According to the structure, complex **4** can be approximately regarded as a linear trimer with $J_{Fe-Mn} = J$ and $J_{Fe-Fe} = 0$. Thus, the Hamiltonian and the Van Vleck expression can be written as

$$\vec{H} = -2J\vec{S}_{Mn}(\vec{S}_{Fe1} + \vec{S}_{Fe2}) \quad (4)$$

$$\chi_M = \frac{Ng^2\beta^2}{4kT} \times \frac{10 + 35e^{7J/kT} + 35e^{5J/kT} + 84e^{12J/kT}}{2 + 3e^{7J/kT} + 3e^{5J/kT} + 4e^{12J/kT}} \quad (5)$$

The magnetic properties of complex **4** can be fitted by a standard least-squares program, and the best fitting parameters were obtained: $g = 2.086(3)$, $J = -3.28(5)$ cm^{-1}, and $R = \sum[(\chi_M T)_{calcd} - (\chi_M T)_{obsd}]^2/\sum(\chi_M T)_{obsd}^2 = 4.8 \times 10^{-4}$. The relatively high Lande factor can be attributed to the orbital contribution of the low-spin Fe^{III} ions. The J value indicates that the cyanide ligand mediates the weak antiferromagnetic coupling between the metal ions in complex **4** because the π pathway with the d_{xz} orbitals of the Mn^{II} and Fe^{III} ions and the p_x orbitals of the C and N atoms in the cyanide ligand provide the dominating magnetic contribution in this complex. The noncompensation of the local interacting spins ($S_{Mn} = 5/2$ and $S_{Fe} = 1/2$) that interact antiferromagnetically through bridging cyanide groups results in the ferrimagnetic behavior for complex **4**.

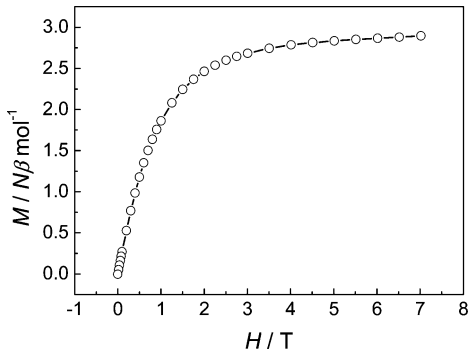

Figure 15. Field dependence of magnetization at 1.8 K for complex **4**. The solid line is a guide for eyes.

In summary, a cyano-bridged heterobimetallic 1D compound, $[(bpca)_2Fe^{III}_2(CN)_6Cu(H_2O)_2 \cdot 1.5H_2O]_n$ (**2**), an unexpected chiral heterobimetallic helical chain complex, $[(bpca)Fe^{III}(CN)_3Cu(bpca)(H_2O) \cdot H_2O]_n$ (**3**), and a trinuclear complex, $[(bpca)_2Fe^{III}_2(CN)_6Mn(CH_3OH)_2(H_2O)_2] \cdot 2H_2O$ (**4**), have been synthesized. Complex **2** displays metamagnetic behavior with a Neel temperature of $T_N = 2.2$ K and a weak critical field of 250 Oe at 1.8 K. Complex **3** exhibits intrachain ferromagnetic coupling between the Cu^{II} and Fe^{III} ions, which presents a typical example of generating a chiral cyano-bridged magnetic compound from achiral materials. Ferrimagnetic behavior was observed in complex **4**. Therefore, $[Fe(bpca)(CN)_3]^-$ is perhaps another versatile building block for the synthesis of the low-dimensional molecule-based magnets by tuning of the coordinated metal ions or solvents.

Acknowledgment. This work was supported by the Major State Basic Research Development Program (G2000077500) and the National Natural Science Foundation of China. The authors thank Prof. Jeffrey R. Long and Dr. Hye Jin Choi for helpful discussions. J.-L.Z. thanks the Program for New Century Excellent Talents at the University of China.

Supporting Information Available: X-ray crystallographic files in CIF format for complexes **2**−**4** and additional characterization data. This material is available free of charge via the Internet at http://pubs.acs.org.

IC0511468